Speciation and organic phase structure in nitric acid extraction with trioctylamine

Srikanth Nayak,*,† Michael J. Servis,† Derrick Combs,† Krystian Szeliga,† and Soenke Seifert‡

†*Chemical Sciences and Engineering Division, Argonne National Laboratory, Lemont, IL 60439*

‡*Advanced Photon Source, Argonne National Laboratory, Lemont, IL 60439*

E-mail: snayak@anl.gov

Abstract

We report on the extraction of nitric acid from its aqueous solutions into organic solutions of trioctylamine (TOA) in toluene, investigated with spectroscopic, X-ray scattering, and computational tools to understand the molecular speciation in the organic phase and its relation to the nanoscale structure of the organic phase. Trends in acid and water extraction clearly show two and three regimes, respectively, but the speciation of nitric acid, water, and the amine in these regimes is not apparent. ^{1}H-NMR of the organic phase shows that there are at least two distinct acidic protons in the organic phase while ATR-FTIR results show that the organic phase with excess acid extraction is a mixture of trioctylammonium-nitrate ion-pairs (TOAH.NO_3), and undissociated nitric acid molecules. IR spectra computed from DFT calculations performed with clusters of undissociated nitric acid molecule hydrogen bonded with the anion of the trioctylammonium nitrate ion-pair are consistent with the ATR-FTIR results. We also show that the chain-like configurations of TOAH.NO_3.HNO_3.H_2O are

favored over TOAH.NO_3.H_2O.HNO_3, i.e., direct interaction between the two extracted nitric acid molecules is more favored compared to a water-mediated interaction. SAXS results of the organic phases were modeled as sums of Ornstein-Zernike scattering and a pre-peak feature at higher Q region, corresponding to features from density fluctuations and extractant packing, respectively. The extraction of undissociated nitric acid by the ion-pairs leads to an increased X-ray scattering contrast in the organic phase without any significant change in the Ornstein-Zernike correlation length. These results show that the organic phase nanostructure is more sensitive to the concentration of TOAH.NO_3 and is relatively unaffected by excess acid extraction. These findings will enable a molecular understanding of the mechanisms behind metal extractions from acidic media with basic extractants.

Introduction

Liquid-liquid extraction, or solvent extraction, is the predominant method of metal separations in nuclear and metallurgical industries, making it a crucial component in the economy of critical metals and the nuclear fuel cycle. Decades of research into the chemistry of solvent extraction has revealed the complexity of the process ranging from the atomic scale, where the electronic structure of the metal dictates metal-ligand binding, to the nanoscale, where weaker intermolecular interactions play a significant role, both of which influence the multicomponent phase equilibrium that governs the separation.[1–8] The delicate balance of these interactions is an active area of research at the confluence of coordination and colloidal chemistry topics.

Metal extractions are typically carried out in highly acidic solutions to ensure solubility of the metal, and to enhance the formation of extractable complexes by providing a high concentration of counteranions. Inorganic acids such as HCl, HNO_3, and H_2SO_4 are commonly used in these separation processes. Anion-specific effects are reported in metal extraction, providing a route for metal-separations, but the mechanisms of such specificity is not under-

stood. Anion-specific factors that can either hinder or promote metal extraction, such as acid and water extractions, aggregation of the extractants, and aqueous/organic speciation of the metal are thought to play a role in this phenomenon.[9–13] Such anion-specificity in metal extraction is observed with different classes of extractants, including solvating-type and anion exchange-type extractants. Acid and water extractions with solvating extractants[13–18] and their influence on metal extraction have been well studied.[19–21] Although amines show similar extraction trends and anion-specificity,[22–24] they have received relatively less attention. Given that the amines are hypothesized to extract metals by anion-exchange mechanism, the effect of acid and water extraction on the extraction and stability of such anionic complexes is of interest. For example, in extraction of hexavalent actinides from HNO_3 using TBP or TOA, there is a maximum in extraction around 6M of aqueous acid.[25,26] In both cases, the dip in extraction at higher acid content is attributed to the competitive extraction of HNO_3, although an alternative explanation involving the formation of inextractable, aqueous nitrate complexes of the metal at high acid concentrations has also been put forward.[27] In the case of TBP, IR spectroscopy and chemical equilibrium modelling studies have been performed to support the competitive nature of acid extraction and have been extended to explain the effect of background salts on extraction.[28–30] Speciation and intermolecular interactions in water-HNO_3-TBP-alkane system have been studied using IR spectroscopy, quantum mechanical calculations, and molecular dynamics simulations showing that water is loosely held in the solution forming hydrogen bonds with other polar solutes that includes a chain-like conformation of TBP.$(HNO_3)_2$.[31–33]

In the context of the anion-exchange mechanism of extraction with amines, it is noteworthy that aqueous solutions of HNO_3 show concentration-dependent speciation, including the formation of ion-pairs.[34] Further, speciation of HNO_3 at aqueous and liquid-liquid surfaces have also been debated and its role in solvent extraction is currently being studied.[35–39] Previously, HNO_3 extraction with tertiary amines in different solvents has been studied showing the formation of ion-pairs, and viscosity and conductivity measurements

have been used to hypothesize the presence of colloidal structures depending on the solvent used.[40–43] Based on conductivity measurements, dipole-dipole interactions and hydrogen bonding have been hypothesized to cause aggregation of the ion-pairs.[44] Cryoscopic and ebullioscopic measurements in these solutions show that the aggregation of the organic species passes through a maxima as the amine concentration is increased, but the data interpretation is limited by the model assumptions.[45] Acid and water extraction trends have been studied with chemical equilibrium models under the assumption of constant aggregation of the organic phase species.[46] Clear pictures of organic phase speciation, the intermolecular interactions, and the resultant organic phase nanostructuring are still lacking. The presence of charged and polar protic species can also cause extensive non-covalent interactions which can affect the nanostructure of the organic phase and metal speciation. Hydrogen bonding networks have been found to be particularly important in nanoscale structuring,[47–49] but in the presence of charged species other interactions can also be significant.[50–53] Aggregation of amine and ammonium-based extractants has been related to metal extraction and separation trends.[12,54,55] This aggregation phenomenon has been principally studied using X-ray and neutron scattering techniques and the data fit to colloidal models, wherein the polar and non-polar species in the organic phase self-assemble into reverse-micellar structures.[12,55] Recently, application of such colloidal models has been challenged, proposing instead that scattering profiles are due to density or concentration fluctuations in the organic phase in the vicinity of its critical point.[33,56,57] Presumably, the two models imply different energetic landscapes with regards to the nanoscale structuring of the organic phase, with differing impacts on metal extraction. Hence, understanding the speciation of the extracted acid, its interactions with other molecules in the organic phase, and the resulting nanoscale structure is essential to understanding the mechanism of metal extraction from acidic solutions with amines.

Here we focus on HNO_3 extraction with TOA to understand the organic phase speciation and nanostructure upon acid extraction. We will be addressing the chemical interactions,

probed by molecular spectroscopy and DFT calculations, that stabilize the organic phase species and relate them to the nanostructure of the organic phase probed by small-angle X-ray scattering. We find that there are two distinct speciations of HNO_3 in the organic phase - at lower acid concentrations all the acid is dissociated, forming trioctylammonium nitrate ion-pairs, and at higher acid concentrations a second undissociated HNO_3 molecule is also present. DFT calculations show shifts in IR frequencies resulting from hydrogen-bonding between the ammonium cation and nitrate, and between nitrate and the undissociated HNO_3 molecule. Water extraction trend shows that there is approximately one water molecule per two TOA even when two HNO_3 molecules are extracted. ATR-FTIR spectra and DFT predicted IR spectra are consistent with the organic phase being a mixture of ion-pairs with or without an associated nitric acid molecule. Water-mediated interaction between the ion-pair and the acid molecule is disfavored compared to direct hydrogen bonding between the ion-pairs and the nitric acid molecule. SAXS results show that the organic phase structure upon the formation of ion-pairs is a combination of liquid structure at larger length scales, showing Ornstein-Zernike scattering, and extractant packing at smaller length scales causing the appearance of a characteristic peak. Colloidal models of the organic phase structure were inadequate to explain the scattering profiles over the range of organic phase compositions. Extraction of excess nitric acid does not significantly affect the solution structure, indicating the non-effect of nitric acid on extended structuring in the organic phase.

Results and discussion

Organic phase composition with HNO_3 extraction

Amines are known to react vigorously with acids, forming ionic ammonium salts. Figure 1(a) shows the variation of total HNO_3 in the organic phase ($[NO_3]_{org}$) obtained by the extraction of HNO_3 with varying concentrations of TOA in toluene. There are two distinct regimes in acid extraction indicating multiple mechanisms. First, there is a rapid rise in acid extraction

when total acid concentration is less than the amine concentration, corresponding to the formation of the trioctylammonium nitrate ion-pairs. Upon completion of this reaction, there is further extraction of HNO_3 into the organic phase, which increases with increasing aqueous HNO_3 and TOA concentrations. At high aqueous HNO_3 concentration a significant quantity of HNO_3 is extracted by toluene itself leading to a slow decomposition of toluene into a bright yellow colored liquid. A linear dependence in aqueous HNO_3 and TOA concentration on the excess HNO_3 extraction into the organic phase, after accounting for the acid extraction by the solvent has been reported as summarized by Bac,[58] and our results align with their findings. However, it is not clear whether the acid extractions by toluene and TOA are related or occur by independent mechanisms.

Water extraction trends with varying HNO_3 and TOA concentrations are shown in Figure 1(b), showing three distinct regimes. The trioctylammonium nitrate ion-pair is more hydrated than the amine. Upon further extraction of HNO_3, water content decreases slightly with a minimum around 4-6 M of initial aqueous HNO_3 concentration. Except at very high HNO_3 concentrations (greater than 8 M), there is ~ 0.5 water per TOA. Given the linear increase in excess acid extraction, the appearance of a minima in water extraction indicates multiple water extraction mechanisms. At high aqueous HNO_3 concentrations, toluene also extracts water (Figure 1(b)) which confounds a clear interpretation of these trends at high acid content. Water extraction at 1:1 TOA:HNO_3 shows a non-linear trend with TOAH.NO_3 concentration as shown in Figure S1, with an initial slope of ~ 0.7. The deviation at higher TOAH.NO_3 concentration could be related to the ion-pair associations in the organic phase, indicating a complex mechanism of water extraction even without excess acid in the organic phase.

Organic phase speciation probed by ^{1}H-NMR

We studied the speciation of TOA and HNO_3 in the organic phase by ^{1}H-NMR and three representative spectra are shown in Figure 2(a,b). Peak shifts associated with the methyl

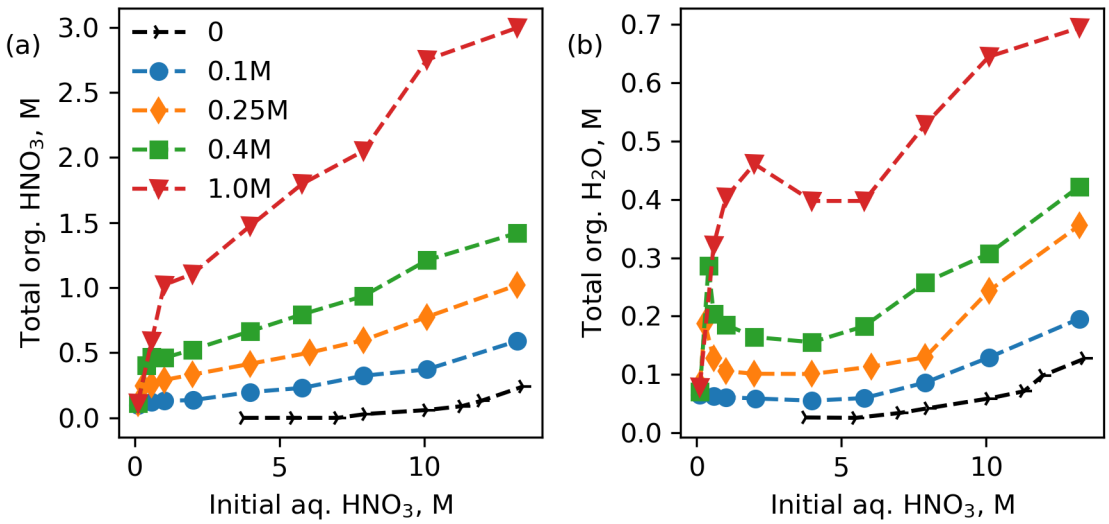

Figure 1: (a) Total concentration of HNO_3 extracted in the organic phases as a function of the initial HNO_3 concentration in the aqueous phase. (b) Concentration of water in the organic phases as a function of initial aqueous HNO_3 concentration, after extraction of HNO_3. Different colors and markers correspond to different concentrations of TOA in toluene. The dashed lines joining the markers are guides for the eye.

and the methylene groups on TOA vary upon acid extraction, with most prominent changes being in the chemical shift of the α-CH_2 group (A in Figure 2). This peak is a triplet in unprotonated TOA and shows a complex splitting pattern with the formation of the protonated TOA, possibly due to the overlap of unprotonated and protonated features. When the concentration of acid extracted is less than that of TOA, there is a broad singlet peak at $\delta > 5$ ppm which gradually moves downfield with increasing acid extraction. We assign this peak (B in Figure 2) to the H-atoms of the ammonium group on $TOAH^+$ that are constantly exchanging with water in the organic phase. Upon extraction of excess acid, a new singlet peak (C in Figure 2) appears in the spectra which we associate with the extraction of the second nitric acid molecule.

Variation of the three labeled chemical shifts in the spectra with $[HNO_3]_{org}$ and the normalized integrals of the peaks corresponding to the acidic protons are shown in Figure 3. When the concentration of extracted acid is less than that of TOA, A and B peaks shift downfield with the formation of $TOAH.NO_3$ ion-pair. The normalized integral under peak

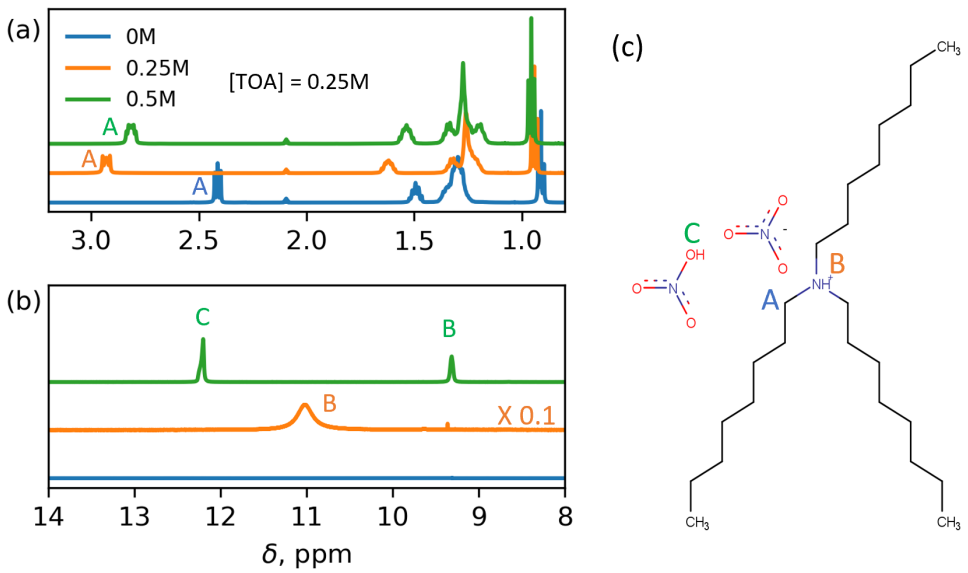

Figure 2: ^{1}H-NMR spectra of organic phases containing 0.25 M TOA and varying amounts of organic nitric acid as labeled in the legend: (a) methyl and methylene protons, and (b) acidic protons. Selected peaks are labelled and identified in the schematic (c). Spectrum corresponding to $[HNO_3]_{org}$ = 0.25 M is scaled up by a factor of 10 to show the feature B clearly. This is a broad peak, possibly due to exchange with water, and the height of the peak is relatively smaller.

B saturates to a value of ∼1 when $[HNO_3]_{org}$ = [TOA]. Upon extraction of excess acid, the C peak moves downfield with increasing excess acid extraction until there is almost 2:1 $[HNO_3]_{org}$:[TOA] after which it shifts upfield. The A and B peaks shift upfield upon increasing acid extraction indicating the effect of excess acid extraction on the TOAH.NO_3 ion-pair. Peak integrals for the B-peak stays around ∼1, consistent with our assignment of the peak to the acidic proton in $TOAH^+$, while those for the C-peak increase with increasing excess acid extraction. Peaks B and C are confounded by the water protons which complicates a direct assignment of the peak integrals to the concentration of different acidic protons. This is apparent in the integral of the C peak being close to ∼1 at almost zero excess acid extraction. Nevertheless, trends in the peak shifts and the integrals clearly show that there are at least two distinct protonated species in the organic phase, aligning with the formation of TOAH.NO_3 ion-pair at lower acid concentrations. They also reflect complex interactions between the extracted species and TOA, but the speciation at higher acid concentrations in

the organic phase is not apparent from these spectra.

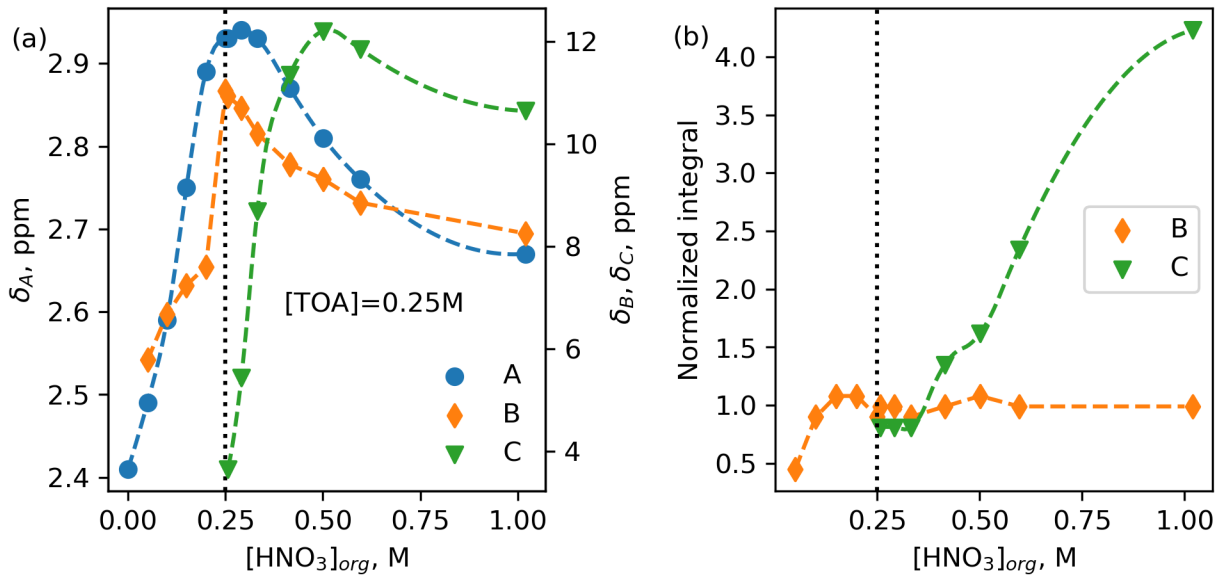

Figure 3: (a) Variation of ^{1}H-NMR peak-shifts with increasing HNO_3 content in the organic phase containing 0.25 M TOA in toluene-D8. A : α-CH_2 groups in TOA or $TOAH^+$, B: proton in $TOAH^+$, and C: proton associated with the second HNO_3 molecule. The dashed lines through the points are only guides to the eye. (b) Variation of the integral under selected peaks in the ^{1}H NMR spectra of the organic phase, normalized per TOA using integral of the terminal methyl protons on TOA. The vertical dotted lines at 0.25 M in (a) and (b) indicate the equivalence point of TOA.

ATR-FTIR and DFT study of TOAH.NO_3 ion-pairs

^{1}H-NMR is an important tool in understanding organic phase speciation due to its general applicability with a variety of extractants and acids. However, as seen in the ^{1}H-NMR results shown above, interpreting the nature of extracted acid is confounded by the presence of co-extracted water. When the acid contains multiple molecular vibrational features that are key signatures of its speciation, vibrational spectroscopy can be very valuable. Vibrational spectroscopy can clearly distinguish between a dissociated (via the vibrational features of nitrate) and an undissociated nitric acid molecule. The speciation of the excess acid can be probed by FTIR spectroscopy, but first we need to understand the spectra of TOAH.NO_3 ion-pairs. So, we conducted ATR-FTIR study to better understand the speciation in the

organic phase after HNO_3 extraction. The ATR-FTIR spectra of trioctylammonium-nitrate ion-pairs (obtained by contacting equimolar TOA and aqueous HNO_3 solutions) at varying concentrations are shown in Figure 4(a). Peaks at 826 cm^{-1}, $\sim$ 1290 cm^{-1}, and $\sim$ 1415 cm^{-1} are attributed to the δ_{2,NO_3^-} and split ν_3 modes of the NO_3^- groups. The spectra around 1040 cm^{-1}, the region corresponding to the ν_1 mode, the symmetric ONO stretching, is also affected by the conversion of the amine to the ammonium nitrate but this region is confounded by the vibrational modes of toluene and TOA. The splitting of the ν_3 mode (asymmetric stretching of the ONO moiety) and the appearance of the ν_1 mode in IR have been attributed to the symmetry breaking of the planar nitrate ion due to hydrogen bonding with the cation ($TOAH^+$).[59,60] While the δ_{2,NO_3^-} peak appears to be relatively unshifted with $TOAH.NO_3$ concentration, the splitting of the ν_3 is decreasing with increasing $TOAH.NO_3$. This could be due to the weakening of the hydrogen bond between the organic cation and the nitrate with increasing $TOAH.NO_3$ concentration due to aggregation of $TOAH.NO_3$.

DFT calculations performed with HNO_3 and tripropylamine show a complete proton transfer to the amine and the formation of hydrogen bond between the tripropylammonium and nitrate. The calculated IR vibrational spectrum for the organic ammonium nitrate is compared with the FTIR of 1M TOA and 1M $TOAH.NO_3$ in figure 4(b). The optimized geometry of the ion-pair is shown in the inset (Figure 4(c)). The predicted spectrum of the ion-pair matches the experimental results reasonably well, but the peaks are relatively blue shifted. This is a common artefact when comparing gas-phase calculations to solutions spectra. Major peaks in the FTIR of $TOAH.NO_3$ and the DFT calculations and their assignments are listed in table 1. The splitting of the ν_3 mode is well reproduced in the calculations.

Water extraction trends show that the ion-pair solutions contain < 1 water per $TOAH.NO_3$ (Figure S1). To probe whether the organic phase contains clusters of $TOAH.NO_3$ with water, we included a water molecule in the DFT calculations and the optimized structure is shown in Figure 4(d) wherein it is hydrogen-bonded to the nitrate. Upon addition of a water

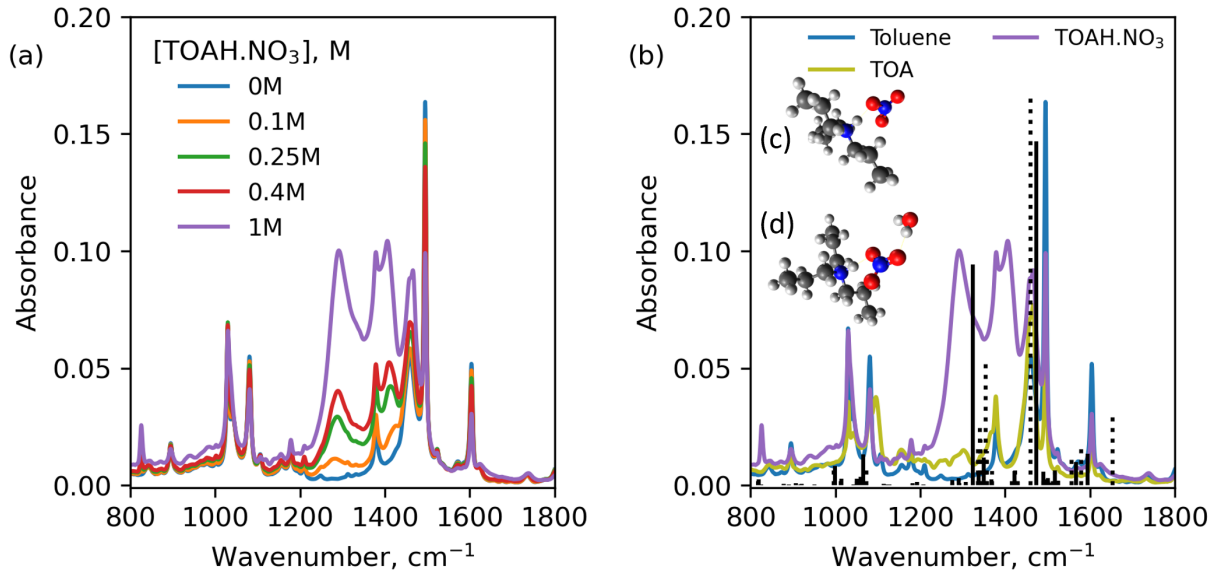

Figure 4: IR spectra of (a) $TOAH.NO_3$ in toluene showing the wavenumber region for the prominent nitrate vibrational modes. Legend entries refer to the concentration of $TOAH.NO_3$ in toluene. (b) Comparison of computed (black vertical bars indicating the position and relative strength of vibrations) and experimental spectra for $TOAH.NO_3$. Experimental results are shown for unprotonated TOA at 1 M and $TOAH.NO_3$ at 1M, both in toluene, whereas the calculations were performed for a tripropylammonium nitrate. The solid black vertical lines are the DFT-predicted peaks for $TOAH.NO_3$ (c), and the dashed vertical lines are the DFT-predicted peaks for $TOAH.NO_3.H_2O$ (d), both in arbitrary units.

molecule solvating the ion-pair ($TOAH.NO_3.H_2O$), the predicted spectra (dashed vertical lines in Figure 4(b)) appear similar to that for the bare ion-pair ($TOAH.NO_3$), with slight frequency shifts. There is an extra peak predicted at 1653 cm^{-1} corresponding to the bending vibration of water, but this peak is not apparent in the experimental results. The OH stretch mode is predicted to be around 3300 cm^{-1}, but this is also absent in the data. Thus, we conclude that $TOAH.NO_3.H_2O$ clusters are not significant in the organic phase when all the TOA molecules are protonated.

When TOA is protonated to form the $TOAH^+$ cation there should be an IR peak corresponding to the N-H stretching mode which can inform about the hydrogen bonding between nitrate and the trioctylammonium cation. The N-H stretching band of trioctylammonium was identified by comparing nitrate salt of TOA with protonated versus deuterated nitric acid solutions and the results are shown in Figure 5(a). The broad feature in the 2000-3000 cm^{-1} region is assigned to the NH stretch which shifts to around 1700-2600 cm^{-1} for the ND stretch. The broadness of the peak is in line with the extensive hydrogen bonding of the protonated amine with the nitrate anions. This broad feature increases with $TOAH.NO_3$ concentration as shown in Figure S2. Gas-phase DFT calculations show a single N-H stretching frequency at 2674 cm^{-1}, well within the experimental result. We probed far-IR region to seek indicators of hydrogen bonding interactions and these spectra show an increasing feature in the 100-200 cm^{-1} region (5(b)), possibly originating from the stretching and bending vibrations of the NH–O hydrogen bond.[61] DFT calculations with $TOAH.NO_3$ show a stretching mode with the cation and the anion vibrating about their mean bond center, indicating multiple energetic contributions to this mode. For the solvated ion-pair $TOAH.NO_3.H_2O$ a peak is predicted at $\sim$ 305 cm^{-1} that corresponds to rocking of the hydrogen-bonded water molecule concomitant with a bending motion of the H_2O–NO_3^- hydrogen bond, but this feature is not apparent in the experimental results.

In summary, the presence of IR characteristic peaks for nitrate, protonated amine, and the absence of characteristic IR peaks for an undissociated HNO_3 at $\sim$950 and $\sim$1650 show that

the extraction of HNO_3 and TOA up to the equimolar concentration lead to the formation of $TOAH^+$-NO_3^- ion-pairs in solution with complete dissociation of HNO_3. Further, there are clear indicators of extensive hydrogen-bonding interactions between the ammonium cation and the nitrate anion. DFT-predicted features associated with ion-pairs being solvated by a water molecule are not apparent in the experimental results. This suggests that the ion-pairs are solvated by other molecules in the solution, possibly by other ion-pairs with aggregation, and agrees with the deviation in water extraction with increasing $TOAH.NO_3$ concentration as shown in Figure S1 .

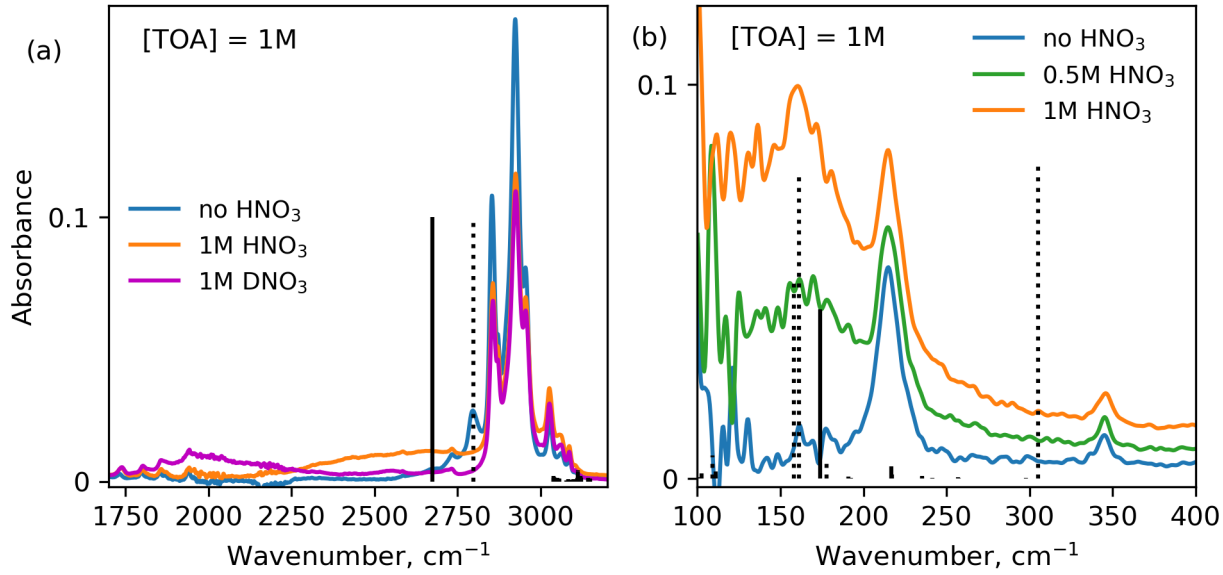

Figure 5: (a)ATR-FTIR of the organic phase with 1M TOA in toluene and after contacting with 1M of HNO_3 or DNO_3, showing the N-H(D) stretching region and the CH stretch region; (b) Far-IR spectra of 1M TOA in toluene before and after contacting with nitric acid, showing the vibrations of the hydrogen bond between the protonated amine and nitrate. The solid, black vertical lines in both the panels are the DFT-predicted peaks for $TOAH.NO_3$, and the dashed vertical lines are the DFT-predicted peaks for $TOAH.NO_3.H_2O$, both in arbitrary units. The legend entries refer to the total concentration of nitric acid extracted into the organic phase.

Aggregation of $TOAH.NO_3$ ion-pairs in toluene

Amines and ammonium salts are hypothesized to be extensively aggregated although the nature of the aggregation is understudied. There are indications of the aggregation effects in water extraction as mentioned above. To understand the nanoscale structure in these solutions we performed SAXS measurements of the organic phase and the resulting SAXS profiles of TOA and the $TOAH.NO_3$ ion-pairs are shown in Figure 6. SAXS of the tertiary amine dissolved in toluene is essentially featureless in the small angle region. At 1M TOA the profile is slightly different at high Q, possibly due to the packing of TOA molecules. SAXS of the $TOAH.NO_3$ ion-pairs, without any significant excess HNO_3, show a much greater variation. At 0.1 M $TOAH.NO_3$ there is mainly an increase in overall scattering without much Q-dependence in the low-Q region. At 0.25 M $TOAH.NO_3$ there is an increase in low-Q scattering, indicating longer length-scale heterogeneity in the sample. This feature is reduced with 0.4 M $TOAH.NO_3$ and is absent in 1 M $TOAH.NO_3$. Concomitant with the reducing low-Q feature, there is an increasing pre-peak feature centered around 0.3 $Å^{-1}$. We have used a sum of Lorentzian centered at Q = 0 $Å^{-1}$ corresponding to Ornstein-Zernike (O-Z) scattering, and a Gaussian peak corresponding to the pre-peak to fit the data, and we refer to the model as the L-G model. Details of the model selection are given in the methods section.

The L-G model corresponds to a fluid made of $TOAH.NO_3$ or its aggregates in toluene with density and/or concentration fluctuations in the vicinity of the critical point of the fluid. Separating structural heterogeneity in such complex fluids arising from density fluctuations and molecular associations as particles is challenging,[62] and it is likely that both contribute to the heterogeneity in the TOA-HNO_3-toluene system as probed by SAXS. As the L-G model provided the best fits to the data, we attribute the low-q scattering to be primarily due to critical fluctuations, i.e., the dynamic heterogeneity. The O-Z correlation length (ξ) is $\sim$ 15.2 Å for 0.25M, and $\sim$ 14.6 Å for 0.4 M of $TOAH.NO_3$ in toluene. At 0.1 M and 1 M of $TOAH.NO_3$, the O-Z scattering is weak and we could not obtain useful

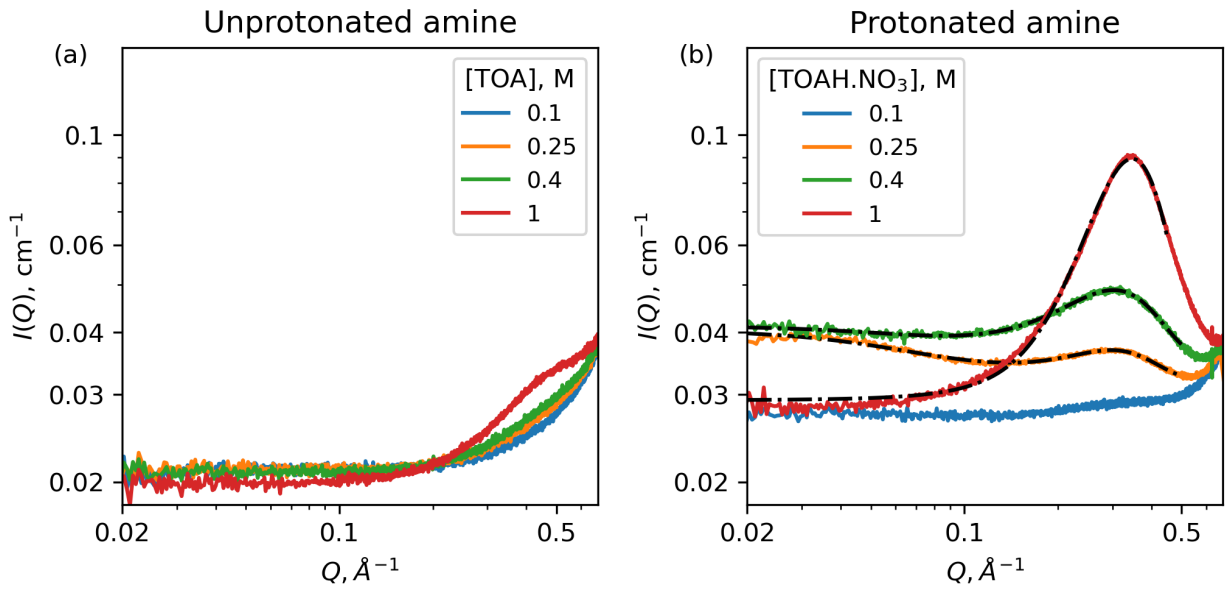

Figure 6: SAXS profiles for (a) binary solutions of TOA in toluene, and (b) TOAH.NO_3 in toluene obtained by near-equimolar reaction of TOA with nitric acid. Legend entries refer to the concentration of TOA or TOAH.NO_3

fits to the L-G model. This behavior of ξ passing through a maximum with the solute concentration corresponds well with the scattering due to critical fluctuations,[57,63,64] with the critical TOAH.NO_3 concentration being between 0.25 and 0.4 M. We note that none of the samples showed phase splitting even at temperatures as low as -19 °C in line with the suppression of phase separation with aromatic solvents. This implies that the theoretical critical temperature is out of the experimentally accessible temperatures and thus we could not ascertain whether the phase behavior of the samples follow the SAXS trends.

In Figure 6(b), the pre-peak is strengthened with increasing TOAH.NO_3 concentration without a significant shift in the peak position. We did not fit the pre-peak region for the 0.1 M TOAH.NO_3 sample as the peak is subdued and significantly affected by the solvent features appearing at >0.5Å^{-1}. The pre-peak is centered at 0.03 Å^{-1} with 0.25 and 0.4 M TOAH.NO_3 and 0.035 Å^{-1} at 1 M TOAH.NO_3. This peak is likely due to the aggregation of TOAH.NO_3 rather than individual TOAH.NO_3 molecules. An approximate measure of the size of TOAH.NO_3 can be obtained as $\sim V_m^{1/3}$ where V_m is the molecular volume obtained

by the density of the solutions ($\sim$ 0.86 to 0.89 g/mL) and assuming ideal mixing, yielding a $d \sim 12$ Å, after including the water contribution. This is less than the length-scale corresponding to the pre-peak, $d = \frac{2\pi}{q} \sim 18 - 21$ Å. This discrepancy suggests that the pre-peak originates from the packing of aggregates of $TOAH.NO_3$. A similar pre-peak feature due to the aggregation of amphiphiles has also been reported in ternary mixtures in water.[65] and in ionic liquid mixtures due to the ordering of ions of the same charge.[66] These results indicate that the solutions of protonated amine salts in toluene are aggregated and show a dynamic and/or structural heterogeneity at larger length-scales.

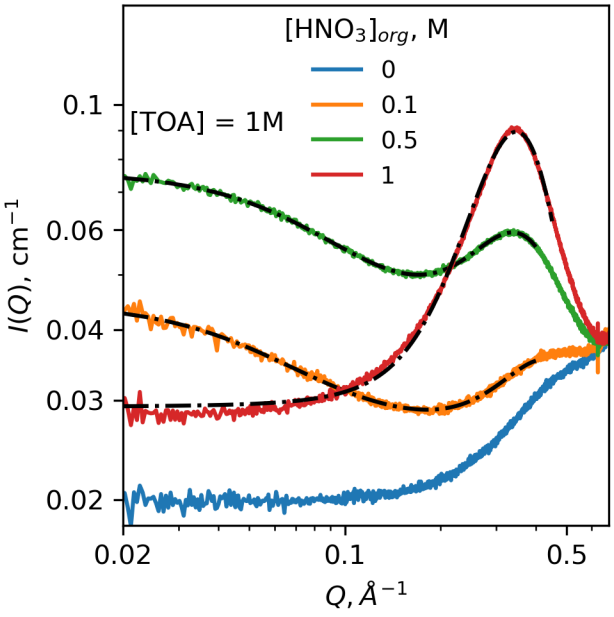

Figure 7: SAXS profiles for 1 M TOA contacted with various concentrations of HNO_3. Legend entries refer to the concentration of HNO_3 in the organic phase

When $[HNO_3]_{org}$ is less than [TOA], the organic is a mixture of TOA and $TOAH.NO_3$ in toluene where TOA can interact with the ion-pairs. Figure 7 shows the SAXS patterns for such mixtures obtained with 1 M TOA where a varying portion of the amines are unprotonated. Interestingly, these mixtures show Ornstein-Zernike scattering depending on the extent of protonation of TOA, indicating that the mixtures of unprotonated amines and the protonated ion-pairs show density fluctuations. The correlation lengths with 0.1 and 0.5 M of $[HNO_3]_{org}$ are 16.3 and 11.0 Å, respectively. The pre-peak feature also depends on the

extent of TOA protonation, increasing with increasing protonation. This suggests enhanced fluctuations exist in the presence of mixtures of protonated and unprotonated TOA, such that full protonation of all TOA suppresses this structuring. More detailed study of these mixtures is needed to understand if this corresponds to a second critical point, or some complicated interplay of ion-pair formation, aggregation, and water extraction.

ATR-FTIR and DFT study of excess HNO_3 extracted with $TOAH.NO_3$

Excess HNO_3 is extracted into the organic phase containing TOA when the aqueous phase HNO_3 concentration exceeds that needed for complete protonation of TOA. At 6M HNO_3 in aqueous phase, the organic phase contains nearly 2 HNO_3 per TOA at all TOA concentrations. FTIR spectra of these organic phases with one excess HNO_3 molecule are shown in Figure 8(a). New peaks appear in the spectra in addition to those identified for $TOAH.NO_3$. There are peaks appearing at 940, 1250, 1330, and 1690 cm^{-1}, and we assign these to vibrational modes of undissociated HNO_3 as listed in Table 1. The peak at 1690 cm^{-1} is assigned to the asymmetric stretch of ONO in undissociated HNO_3 as this peak is not detected in $TOAH.NO_3$ without excess HNO_3 (Figure 4).

DFT optimized geometries for $TOAH.NO_3$ and HNO_3 (Figure 10(c)) and the predicted IR spectra also show that the second HNO_3 is undissociated in the organic phase and is interacting primarily with the nitrate anion of the ion-pair via a hydrogen bond between the proton of the undissociated HNO_3 and the oxygen of the nitrate anion. Interestingly, in the case of excess HNO_3 extraction with TBP, two peaks are observed in this region, attributed to the first and second HNO_3 molecules with the latter being hydrogen bonded to the former in a chain-like conformation.[31,32] In contrast, with TOA the first HNO_3 molecule is completely dissociated and the second HNO_3 molecule is undissociated and hydrogen bonded to the nitrate.

The peaks corresponding to the nitrate anion associated with the $TOAH^+$ also show interesting changes with the extraction of excess HNO_3. The out-of-plane bending mode

of nitrate, δ_{2,NO_3^-} gets red-shifted, shifting by around 8 cm^{-1}. The asymmetric stretching mode (ν_3) of the nitrate also changes, with the 1420 cm^{-1} peak diminishing and the 1290 cm^{-1} peak red shifting to 1250 cm^{-1} with increasing acid extraction. These changes in the vibrational modes corresponding to the nitrate anion also show that the second HNO_3 molecule is interacting with the nitrate anion bound to the protonated TOA. The calculated spectra are also qualitatively consistent with the experimental results, as shown in Figure 8(b).

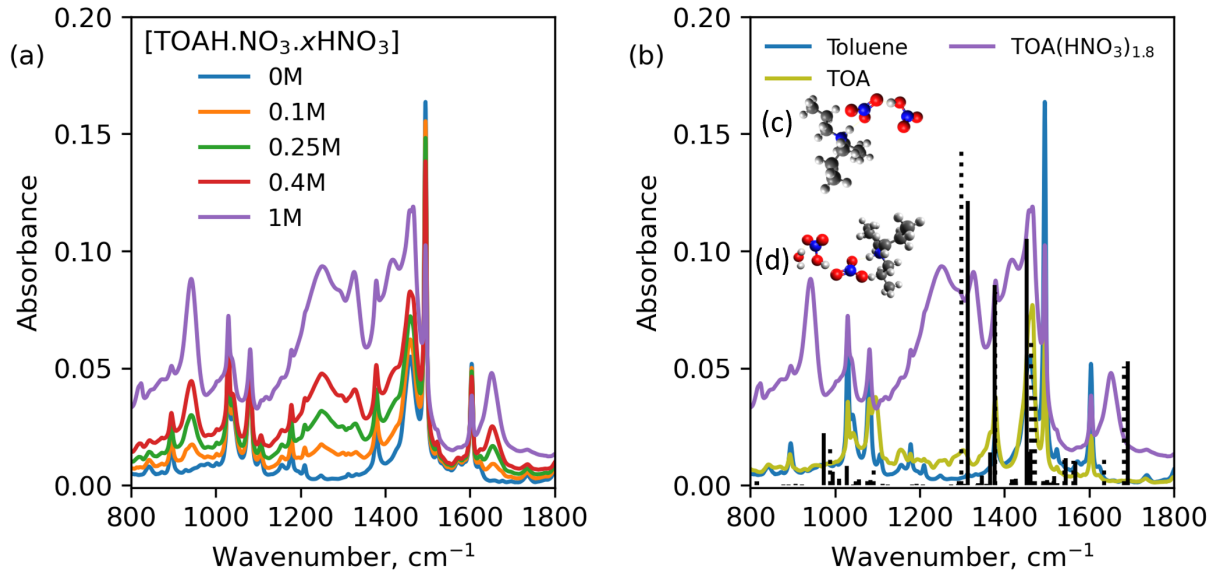

Figure 8: IR spectra of (a) Excess HNO_3 with $TOAH.NO_3$ in toluene showing the wavenumber region for the prominent NO_3^- and HNO_3 vibrational modes. Legend entries refer to the concentration of $TOAH.NO_3.xHNO_3$, where x is nearly 1. The samples were obtained by equilibrating TOA solutions with 6M of aqueous HNO_3 and the final organic phase was found to contain a total of nearly 2 HNO_3 per TOA (1), i.e., approximately one excess HNO_3 molecule per $TOAH.NO_3$ ion-pair . (b) Comparison of the computed (black vertical bars indicating the position and relative strength of vibrations) and experimental spectra for $TOAH.NO_3$. Experimental results are shown for unprotonated 1M TOA and 1M $TOAH.NO_3$ with an excess of $x \sim 0.8$M HNO_3, both in toluene, whereas the calculations were performed for a tripropylammonium nitrate. The solid, black vertical lines are the DFT-predicted peaks for $TOAH.NO_3.HNO_3$, and the dashed vertical lines are the DFT-predicted peaks for $TOAH.NO_3.HNO_3.H_2O$, both in arbitrary units

There is nearly one water molecule per two $TOAH.NO_3$ in the organic phase when extracting from 6M HNO_3, raising the possibility that some of the $TOAH.NO_3$ ion-pairs, or the

undissociated $HNO_{3,org}$ molecules, are hydrated. When HNO_3 is hydrated the N-OH stretching and the NO-H bending are expected to be blue-shifted to 990 cm^{-1} and $\sim$ 1400 cm^{-1}, respectively.[67,68] Our result indicates that the undissociated HNO_3 extracted into the organic phase is not significantly hydrated. This is also confirmed by DFT calculations as follows. Given 1:2 water:TOA composition in the organic phase, the organic phase can be considered as a mixture of $TOAH.NO_3.HNO_3$ with and without a water molecule. There are two main configurations for including a water molecule in $TOAH.NO_3.HNO_3$: $TOAH.NO_3.HNO_3.H_2O$ or $TOAH.NO_3.H_2O.HNO_3$, i.e., the ion-pair $TOAH.NO_3$ interacting with the second HNO_3 directly or mediated by water. These configurations are represented in Figure 9(a) and (b). Optimized structures obtained by DFT calculations for the two configurations are shown in Figure 9(d) and (e), respectively, and the predicted IR spectra are shown alongside the experimental results in Figure 9(c). We note that the IR spectra predicted by DFT for $TOAH.NO_3.HNO_3$ and $TOAH.NO_3.HNO_3.H_2O$ are very similar to each other, with differences being only in small shifts in peak positions and the appearance of intramolecular vibrations of water (Figure 8(b)). In fact, the interaction between the second nitric acid molecule and water appears to be weaker than the nitrate-nitric acid interaction based on the distance between the hydrogen bond donors and acceptors . However, these are gas-phase calculations and the solvation and aggregation present in these solutions may play a role in stabilizing the extracted water molecule as well.

The $TOAH.NO_3.H_2O.HNO_3$ configuration shows a significantly different spectra (Figure 9(c)), with peaks corresponding to combined vibrations of water and the second nitric acid molecule appearing at $\sim$ 849.5 and $\sim$ 1188 cm^{-1}. The OH stretch of the second nitric acid molecule is predicted to be at $\sim$ 2413.6 cm^{-1}. As these features do not match the experimental data, we eliminate the $TOAH.NO_3.H_2O.HNO_3$ shown in Figure 9(b) as a significant species in the organic phase. From these results we infer that the dominant species in the organic phase upon excess acid extraction are $TOAH.NO_3$, $TOAH.NO_3.HNO_3$, and $TOAH.NO_3.HNO_3.H_2O$. This is in contrast to the water-mediated extractant-acid interac-

tion proposed for HNO_3 extraction with malonamides.[69]

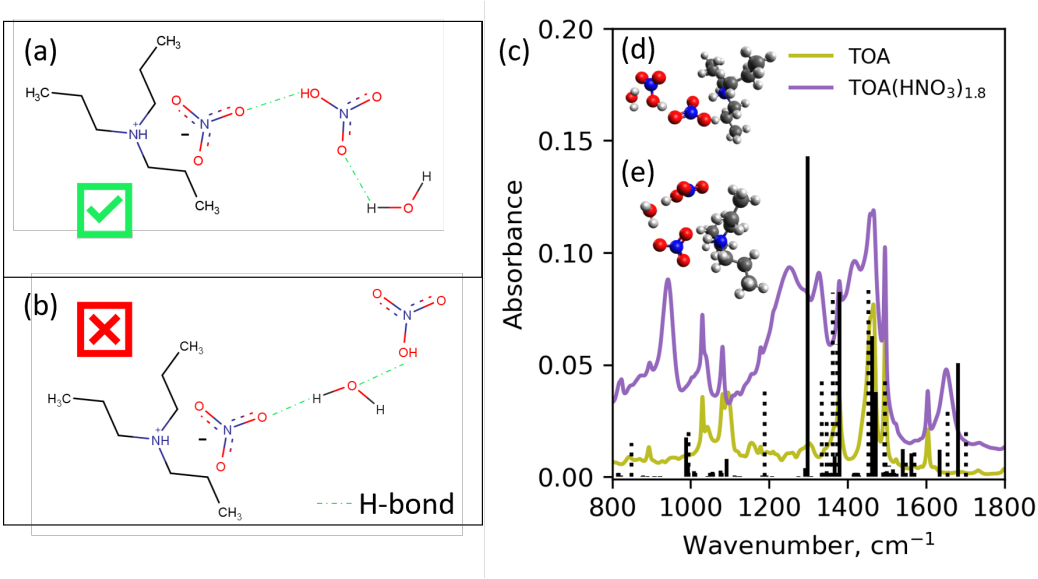

Figure 9: (a,b) Possible interaction modes of water and nitric acid with $TOAH.NO_3$ shown with hydrogen-bonds based on DFT calculations, (c) predicted IR spectra for the two modes shown in a and b, along with experimental ATR-FTIR results for 1 M TOA without any $HNO_{3,org}$ and with a total of 1.8 M $HNO_{3,org}$, i.e., 0.8M of excess acid. (d, e) DFT-optimized geometries for a and b configurations. The solid, black vertical lines are the DFT-predicted peaks for $TOAH.NO_3.HNO_3.H_2O$, and the dashed vertical lines are the DFT-predicted peaks for $TOAH.NO_3.H_2O.HNO_3$, both in arbitrary units

Figure 10 shows the FTIR spectra for the organic phases as a function of amine and excess nitric acid concentration. In all the sub-panels, spectral signatures of undissociated HNO_3 increase monotonically with increasing acid extraction. The extra peaks appearing at 1300 cm^{-1} and 1675 cm^{-1} at high acid concentrations are due to HNO_3 extracted by toluene as shown in Figure S3. These results show that throughout the concentration ranges of HNO_3 and TOA the dominant species in the organic phase are limited to TOA, $TOAH.NO_3$, and $TOAH.NO_3.HNO_3$, with water possibly interacting with the nitrate or the HNO_3 in a peripheral manner.

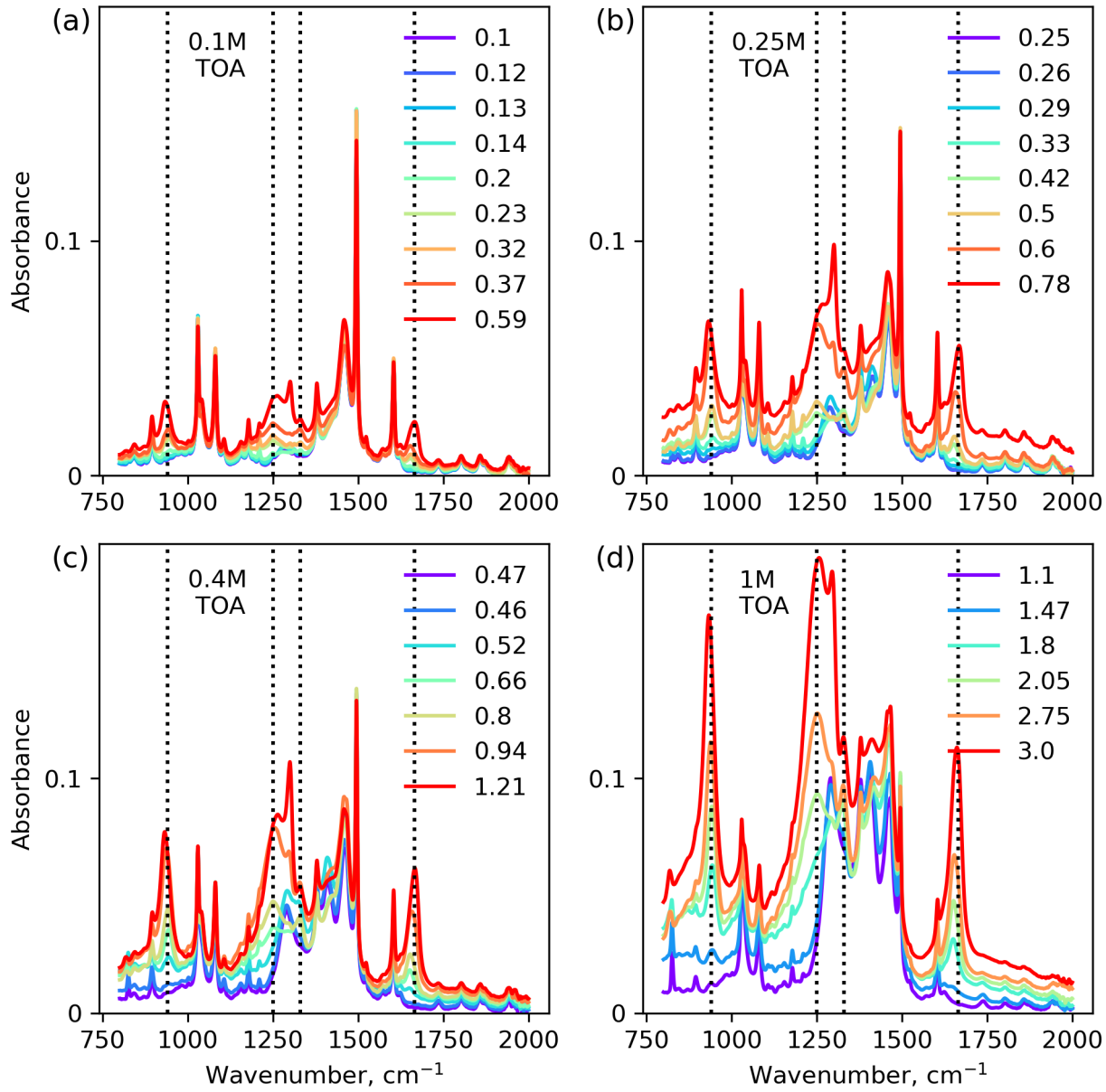

Figure 10: ATR-FTIR spectra of TOAH.NO_3 with excess HNO_3 extraction showing the prominent peaks corresponding to vibrational modes of NO_3^- and HNO_3 in the organic phase. The four subpanels correspond to the four TOA concentrations studied here. The dotted lines in the subpanels are placed at 940 cm^{-1} and 1665 cm^{-1}, corresponding to undissociated HNO_3 vibrations, and 1250 cm^{-1} and 1330 cm^{-1}, corresponding to NO_3^- vibrations. The legend entries correspond to the total $[HNO_3]_{orgz}$.

Table 1: Experimental and calculated IR-active vibrational modes of trioctylammonium nitrate and the excess HNO_3 in toluene. Features obscured by signals from TOA and toluene are labeled as obscured in the table. Abbreviations: "na" = not applicable, expt = experimental, calc = calculated by DFT methods.

Description	**TOAH.NO_3, calc**	**TOAH.NO_3, expt**	**TOA.2HNO_3, calc**	**TOA.2HNO_3, expt**
TOAH—NO_3 stretch	173.9	$\sim$ 170	179.8	$\sim$ 170
$TOAHNO_3$—HNO_3 stretch	na	na	210.5	obscured
ONO in-plane bending	713.1	obscured	711.6, 720.4	obscured
NO_3^- out-of-plane bending (δ_{2,NO_3^-})	818.8	826	816	818
NO_3^- out-of-plane bend, 2nd HNO_3	na	na	784.8	770, 785
ONO—OH stretch	na	na	973.3	940
NO–H bending	na	na	1027.9	1330
NO_3^- symmetric stretch (ν_1)	1065	obscured	1083.9	obscured
ONO asymmetric stretch (ν_3)	1323.3, 1349, 1473.9	1290, 1420	1313, 1376.4, 1452.4, 1461.8	1250, 1330, 1420
NH in-plane bend	1567.6	obscured	1544.3	obscured
NH out-of-plane bend	1594.3	obscured	1567	obscured
ONOH asymmetric stretch	na	na	1690	1650
NH stretching	2674	2000-3000	2916	obscured
OH stretch (HNO_3)	na	na	2743.7	obscured

SAXS study of aggregation of TOAH.NO_3 with excess acid extraction

Having established the major speciation in the organic phase upon excess acid extraction, we now turn to the aggregation of the TOAH.NO_3.HNO_3 species in the organic phase. Increasing the concentration of polar solutes in a non-polar liquid can be expected to cause changes in the nanoscale structure of the fluid. We probe this using SAXS and the results for organic phases with increasing HNO_3 content obtained by the excess acid extraction is shown in Figure 11 along with the fits obtained by the L-G model (equation 3). At all four TOAH.NO_3 concentrations, increasing acid extraction appears to significantly affect the

low-q scattering and, to a lesser extent, the pre-peak. At all TOA concentrations $I(q = 0)$ increases with increasing excess acid content, although we cannot ascertain this at 1M TOA where the OZ scattering is too weak to be fit. The fit parameters for the SAXS patterns shown in Figure 11 are shown in Figure 12.

We could not obtain reliable fits for the 0.1 M TOA samples as the pre-peak feature is not easily distinguished from the background, and this in turn affects fitting the low-Q scattering. We found that the correlation length, ξ, in particular is very sensitive to the choice of fitting range, and has a high error estimated from the fits, even larger than the fit value itself. L-G model fits to the 0.1M TOA-HNO_3 data at various fixed ξ values are shown in Figure S5, showing that ξ values above 12 Å produce good fits to the data. Trends in the variation of I_0 are not affected by the choice of fixed ξ value (Figure S6). The fact that we get reliable fit values for I_0, but not ξ indicates that I_0 is affected by factors other than critical fluctuation, namely enhanced contrast due to the extracted nitric acid molecules. All the other samples with higher concentrations of TOA were fit with all the model parameters being free to vary.

Variation in all the parameters can be broadly divided into two regimes: one where the organic phase is a mixture of the amine and its protonated salt, and another where the amines are completely protonated and there is a gradual excess acid extraction. The first regime was briefly discussed in the previous section (Figure 7). Since most of the data was obtained with excess acid extraction, we focus on the second regime. Here both TOAH.NO_3 concentration and excess acid concentration significantly affect the nanoscale structure of the fluid. I_0 appears to have a maximum between 0.25M and 0.4M ($\sim$ 0.1 to 0.17 volume fraction of TOAH.NO_3), which is lower than the corresponding extractant concentration for neutral extractants such as TBP and DMDPMA in the absence of acid.[57,63,64] The origins of this difference is not clear, but it could be characteristic of TOA, the presence of acid, or some combination thereof.

With increasing excess acid extraction, ξ does not vary significantly while the I_0 increases

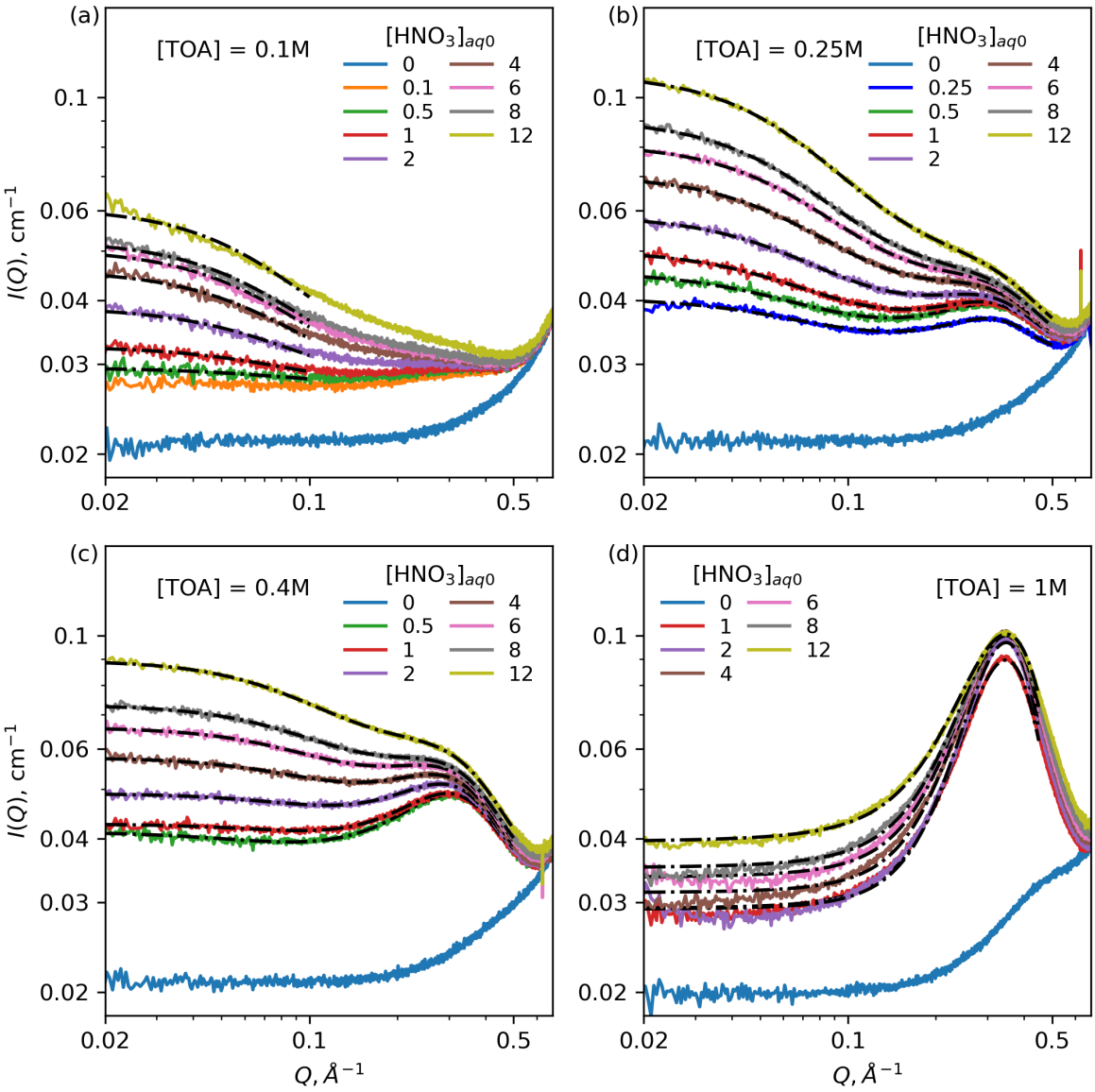

Figure 11: SAXS data for various concentrations of TOA equilibrated with varying concentrations of nitric acid - (a) 0.1 M TOA, (b) 0.25 M TOA, (c) 0.4 M TOA, and (d) 1 M TOA in toluene. Legend entries refer to the initial HNO_3 concentration in the aqueous phase ($[HNO_3]_{aq0}$). Black solid traces in all the panels are fits to the data obtained using the L-G model (equation 3). Fits to the 0.1M TOA dataset in panel (a) were obtained with a fixed correlation length of 12 Å.

monotonically with organic acid content. This indicates that the excess acid extracted mainly increases the scattering contrast and not the nanoscale structure of the fluid. Given that the solutions are far from the critical point (as we did not observe any phase separation at temperatures as low as -19 °C), a change in ξ due to the effect of extracted acid on T_c would be slight.[57] Similarly, change in I_0 due to a change in T_c would be slight, but it can be significantly affected by the change in scattering contrast. Similar phenomena is observed with binary mixtures of alcohols and toluene where an interplay of density and concentration fluctuations (clustering) was hypothesized to affect the I_0 and correlation length differently.[70] We also note that there is no distinguishing feature corresponding to the excess nitric acid extracted with toluene, again reinforcing the fact that excess acid mainly increases the scattering contrast regardless of the specific interactions it has in the organic phase. Similar phenomenon is reported with nitric acid extraction with diglycolamides, where extracted acid disrupts hydrogen-bonding networks,[48] and is also reminiscent of the SAXS features in quaternary ammonium nitrate solutions.[12]

The pre-peak feature also shows a dependence on TOAH.NO_3 and excess acid concentration. The trends in pre-peak amplitude and center with increasing excess acid extraction differ for 1 M TOAH.NO_3 from those for 0.25 and 0.4 M TOAH.NO3. There is no apparent pre-peak feature for 0.1 M TOAH.NO_3 solutions. For 0.25 and 0.4 M TOAH.NO_3, the pre-peak amplitude increases slightly with acid concentration while the pre-peak position decreases, suggesting a swelling of the aggregates. At 1 M TOAH.NO_3 with increasing excess acid concentration the amplitude of the pre-peak slightly decreases but position does not change. These trends could be rationalized by considering that the scattering contrast in these fluids is reversed at 1 M of TOAH.NO_3, and increasing HNO_3 in the fluid decreases the concentration of the scatterers, but more studies are needed to understand the nature of these aggregates. Role of extracted water in the nanoscale structure of these organic phases is also unclear. In solvating extractants water is found to facilitate extend hydrogen-bonded networks, leading to the formation of long-range structures.[32,48,49] However, here there is

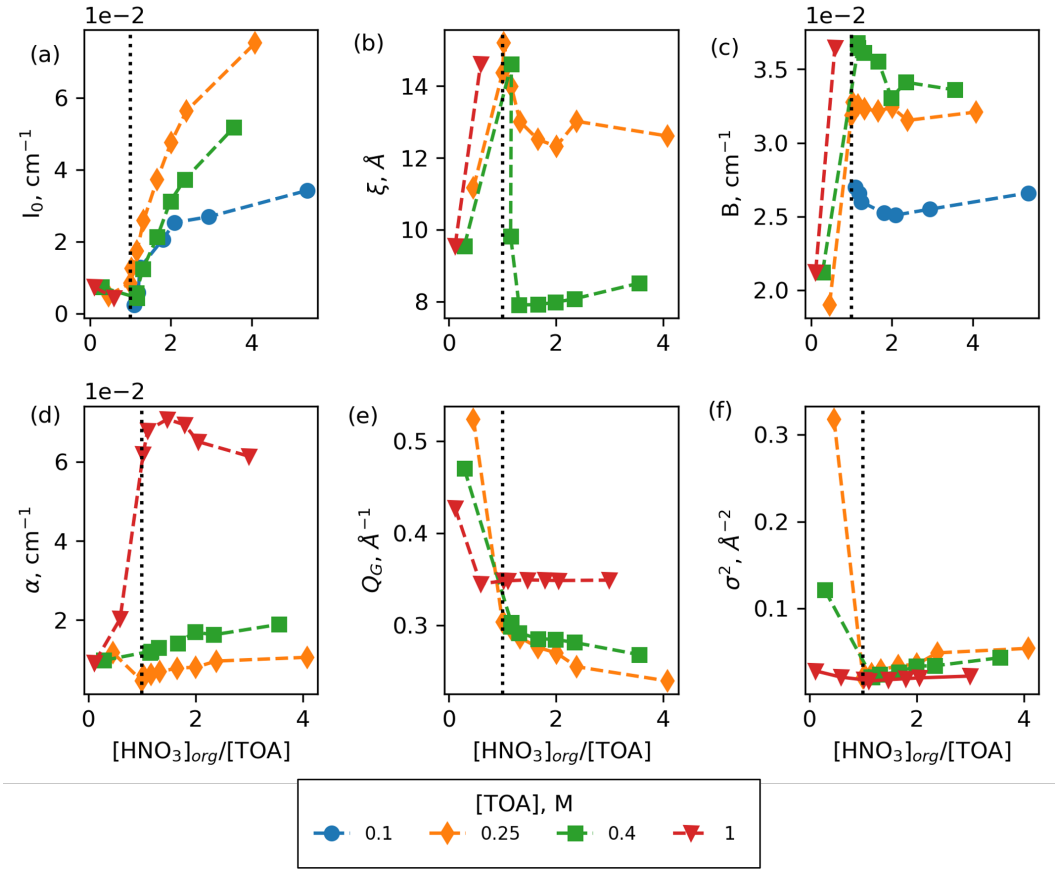

Figure 12: Variation of the parameters obtained from fitting the SAXS data shown in Figure 11 with the L-G model. Panels (a), (b), and (c) show the variation of I_0, correlation length, and the background terms in the fits. Panels (d), (e), and (f) show the variation of the pre-peak amplitude, center, and width in the fits. The x-axis is the total nitric acid extracted into the organic phase ($[HNO_3]_{org}$) divided by the concentration of TOA. The dotted line in each of the panels refers to x = 1 where the amine is completely protonated. Values to the left of this line correspond to mixtures of TOA and TOAH.NO_3 (SAXS data in Figure 6 and Figure 7), and to the right are the solutions with excess acid extraction (refer to SAXS data in Figure 11). Markers (colors) of the scatter data in the three panels correspond to different concentrations of TOA in the organic phase - circle (blue): 0.1 M TOA, diamond (orange): 0.25 M TOA, square (green): 0.4 M TOA, and triangle (red): 1 M TOA.

no clear trend in the relationship between the organic phase structure and water content (Figure S7). This indicates that the organic phase structure is driven mainly by extractant and acid molecules, aligning with the weak association of water with the ion-pairs as seen in the previous sections.

Conclusions

Using a combination of analytical, spectroscopic, X-ray scattering, and computational techniques, we have investigated the speciation of HNO_3 in the organic phase after extraction with TOA in toluene and the resulting changes in the nanoscale structure of the organic phase. Acid and water extraction trends show multiple extraction regimes, and we have demonstrated the existence two distinct speciation of extracted HNO_3, first as a dissociated acid leading to the formation of trioctylammonium nitrate ion-pair, and second as an undissociated HNO_3 molecule hydrogen bonded to the nitrate. Solvating extractants like TBP also show similar acid and water extraction trends, but acids appear to be undissociated throughout the extraction regime. While ^{1}H-NMR spectroscopy shows the presence of multiple acidic species in the organic phase with TOA, ATR-FTIR spectroscopy, in combination with electronic structure calculations provides a clearer picture of the speciation of the acid. Water appears to be loosely bound to the ion-pairs and the undissociated HNO_3 molecules with the ion-pairs preferring to form hydrogen bonds with the undissociated HNO_3 rather than with water. Modelling of the SAXS data across the organic phase compositional space show that the organic phase structure is a combination of liquid structure at larger length scales, described by the Ornstein-Zernike scattering equation, and extractant packing as aggregates. SAXS behavior with respect to the concentration of ion-pairs of protonated amines resembles scattering due to critical fluctuations. Interestingly, an increase in hydrogen bonding moieties with increasing excess acid extraction did not significantly change the Ornstein-Zernike correlation length. The pre-peak feature, assigned to aggregates of the

ion-pairs, shows a complicated trend with acid extraction, depending on the concentration of the ion-pairs in solution. These findings show that the acid extraction uniquely affects speciation and nanoscale structure with basic extractants. Mechanism of water extraction and its role in metal extraction is still not easily explained. In light of our results, the role of non-covalent interactions including ion-ion interactions, hydrogen bonding, and ion-dipole interactions in metal extraction with basic extractants need further study. Differences in such non-covalent interactions can play a role in separation of metals as anionic complexes with these basic extractants.

Experimental

Tri-n-octylamine (TOA), D_2O (99 atom% D), concentrated DNO_3, and toluene were purchased from Millipore-Sigma Aldrich LLC. Concentrated HNO_3 was purchased from Fisher Chemicals. All the chemicals were used as received without any purification. HNO_3 solutions were prepared by volumetric dilutions of concentrated HNO_3. TOA solutions in toluene were prepared by dissolving a known mass of TOA in toluene in volumetric flasks. Acid extractions were conducted in glass tubes with phenolic caps by contacting equal volumes of aqueous HNO_3 solutions and organic TOA solutions. The two liquid phases were contacted for five minutes and separated by centrifugation. The phases were then manually separated with plastic pipettes for further analysis. All the samples were prepared under ambient conditions of T = 20 °C.

Extraction of HNO_3 was studied potentiometrically. The aqueous solution was diluted with deionized water and the pH was measured, both before and after extraction. Water extraction was studied by measuring the concentration of dissolved water in the organic phase after acid extraction by the coulometric Karl Fisher method. Densities of the organic solutions were measured with the help of a calibrated balance with a 0.1 mg precision.

Samples for ^{1}H-NMR measurements were made with deuterated toluene. ^{1}H-NMR spec-

tra were recorded on a 500 MHz Bruker spectrometer. All the spectra were referenced to the toluene peak in the uncontacted TOA-toluene(D8) solution. ATR-FTIR measurements were performed on a Nicolet iS50 FTIR spectrometer equipped with an diamond crystal - ATR accessory. A small droplet of the sample was placed on the ATR crystal and covered with a plastic cup to prevent evaporative losses during measurement. An air background was measured and subtracted from the sample spectra. All measurements were averaged over 32 scans with zero-fill factor.

Small-angle X-ray scattering measurements were conducted at Sector 12-ID-C beamline of Advanced Photon Source, Argonne National Laboratory with a Pilatus 2M detector having a pixel size of 0.173 mm. Following parameters were used in obtaining the SAXS data: incident photon energy = 12 keV, sample to detector distance = 2206 mm, and the exposure time = 1 s. The samples were held in a 1.5 mm outer-diameter quartz capillary. Same capillary was used for all the samples to keep a constant capillary background and sample thickness. Five shots were collected per sample to improve the data statistics. Air background was measured to obtain the background scattering and water scattering was used for intensity calibration. The capillary was rinsed multiple times with a soap solution and water in between the samples. The 2-D data were processed at the beamline using standard procedures to obtain 1-D averaged scattering profiles.

SAXS model selection

We tested three models: (a) Tuebner-Strey model (T-S, equation 1) which is used in describing the structure of microemulsions,[71] (b) a sum of Guinier scattering and a Gaussian peak to describe the low-q features and the pre-peak, respectively (G-G model, equation 2), and (c) a sum of Ornstein-Zernike scattering (Lorentzian centered at q=0) and a Gaussian peak to describe the low-q feature and the pre-peak (L-G model, equation 3). Ornstein-Zernike shape is used to describe the dynamic fluid structure due to thermal fluctuations while the Guinier shape is generally used to describe SAXS from dilute solutions of particles with

ill-defined shapes but possessing a characteristic length scale called the radius of gyration. A comparison of the fits obtained by the three models is shown in Figure 13 with the SAXS data for 0.25 M TOA equilibrated with $\sim$ 12 M HNO_3. For all the conditions studied in this article the L-G model lead to best fits with the least reduced chi-squared values. Equations for the different models are as below.

Teubner-Strey model (T-S):

$$I(Q) = \frac{1}{a + c_1 Q^2 + c_2 Q^4} + B \tag{1}$$

Guinier-Gaussian model (G-G):

$$I(Q) = I_0 e^{-(Q\xi)^2} + \alpha e^{\frac{-(Q-Q_G)^2}{\sigma^2}} + B \tag{2}$$

Lorentzian-Gaussian model (L-G):

$$I(Q) = \frac{I_0}{1 + (Q\xi)^2} + \alpha e^{\frac{-(Q-Q_G)^2}{\sigma^2}} + B \tag{3}$$

T-S model was the worst performing model of the three, possibly because it simultaneously fits the low-Q and the pre-peak features whereas the other two models are more flexible and additively decouple the low-Q feature from the pre-peak feature. Best fits to the data using the T-S model are shown in Figure S4, wherein it is clear that this model does not adequately capture the trends in the organic phase SAXS. The G-G model performs well for most of the samples, except for those with a high low-Q scattering. The G-G model can be thought of as corresponding to a large cluster with the pre-peak describing the internal packing of the constituents in the cluster (either the TOA.HNO_3 molecules or their molecular aggregates). Based on this analysis we have chosen the L-G model to describe the SAXS data.

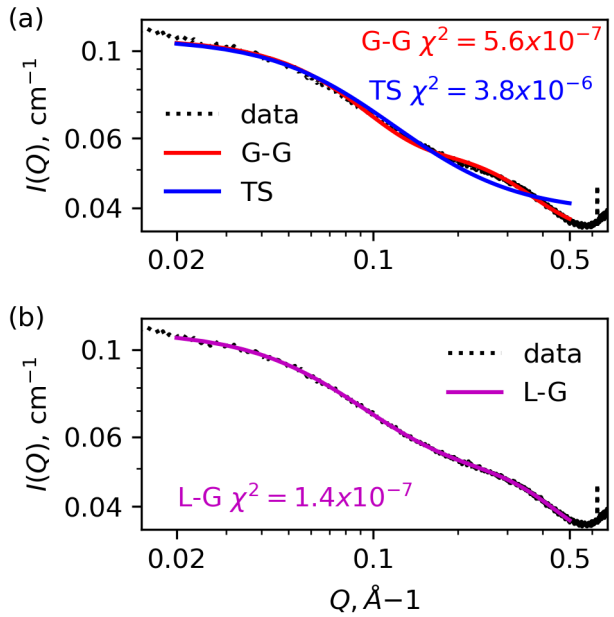

Figure 13: Comparison of different models used to fit the SAXS data for 0.25M TOA equilibrated with 12M nitric acid. Panel (a) shows the experimental data in dotted line, a combination of Guinier and Gaussian peak (red trace), fit obtained with Teubner-Strey model for microemulsions (blue trace), and (b) the fit obtained with the Lorentz-Gaussian model. The reduced chi-squared values associated with the fits are shown in the subpanels. L-G model was found to produce the best fits for the SAXS data

Computational

Cluster geometries were optimized with density functional theory (DFT) using the B3LYP functional and 6-31+G(d,p) basis set, followed by a frequency calculation. Solvent effects of toluene were modeled using the conductor-like polarizable continuum model. All DFT calculations were performed in Gaussian 16.[72]

Acknowledgement

This work was supported by the U.S. Department of Energy, Office of Basic Energy Science, Division of Chemical Sciences, Geosciences, and Biosciences, Separation Science program under contract DE-AC02-06CH11357. Use of the Advanced Photon Source, an Office of Science User Facility operated for the U.S. Department of Energy (DOE) Office of Science by Argonne National Laboratory, was supported by the U.S. DOE under Contract No. DE-AC02-06CH11357. We gratefully acknowledge the computing resources provided on Bebop, a high-performance computing cluster operated by the Laboratory Computing Resource Center at Argonne National Laboratory.

Supporting Information Available

Supporting Information contains the following:

- Water extraction by TOAH.NO_3 ion-pairs
- Additional ATR-FTIR results
- Additional SAXS fitting results
- Principal components analysis of the ATR-FTIR data

References

(1) Nash, K. L. A review of the basic chemistry and recent developments in trivalent f-elements separations. *Solvent Extraction and Ion Exchange* **1993**, *11*, 729–768.

(2) Wilson, A. M.; Bailey, P. J.; Tasker, P. A.; Turkington, J. R.; Grant, R. A.; Love, J. B. Solvent extraction: the coordination chemistry behind extractive metallurgy. *Chemical Society Reviews* **2014**, *43*, 123–134.

(3) Baird, M. Solvent extraction—the challenges of a "mature" technology. *The Canadian Journal of Chemical Engineering* **1991**, *69*, 1287–1301.

(4) Li, Z.; Dewulf, B.; Binnemans, K. Nonaqueous solvent extraction for enhanced metal separations: concept, systems, and mechanisms. *Industrial & Engineering Chemistry Research* **2021**, *60*, 17285–17302.

(5) El-Nadi, Y. Solvent extraction and its applications on ore processing and recovery of metals: classical approach. *Separation & Purification Reviews* **2017**, *46*, 195–215.

(6) Al Zoubi, W. Solvent extraction of metal ions by use of Schiff bases. *Journal of Coordination Chemistry* **2013**, *66*, 2264–2289.

(7) Geist, A.; Adnet, J.-M.; Bourg, S.; Ekberg, C.; Galán, H.; Guilbaud, P.; Miguirditchian, M.; Modolo, G.; Rhodes, C.; Taylor, R. An overview of solvent extraction processes developed in Europe for advanced nuclear fuel recycling, part 1—Heterogeneous recycling. *Separation science and technology* **2021**, *56*, 1866–1881.

(8) Moyer, B. A. *Ion exchange and solvent extraction: Volume 23, Changing the landscape in solvent extraction*; CRC Press, 2019; Vol. 23.

(9) Chiarizia, R.; Briand, A. Third phase formation in the extraction of inorganic acids by TBP in n-octane. *Solvent Extraction and Ion Exchange* **2007**, *25*, 351–371.

(10) Dejugnat, C.; Berthon, L.; Dubois, V.; Meridiano, Y.; Dourdain, S.; Guillaumont, D.; Pellet-Rostaing, S.; Zemb, T. Liquid-liquid extraction of acids and water by a malonamide: I-anion specific effects on the polar core microstructure of the aggregated malonamide. *Solvent Extraction and Ion Exchange* **2014**, *32*, 601–619.

(11) Dourdain, S.; Déjugnat, C.; Berthon, L.; Dubois, V.; Pellet-Rostaing, S.; Dufrêche, J.-F.; Zemb, T. Liquid-liquid extraction of acids by a malonamide: II-anion specific effects in the aggregate-enhanced extraction isotherms. *Solvent Extraction and Ion Exchange* **2014**, *32*, 620–636.

(12) Nayak, S.; Lovering, K.; Uysal, A. Ion-specific clustering of metal–amphiphile complexes in rare earth separations. *Nanoscale* **2020**, *12*, 20202–20210.

(13) Peroutka, A. A.; Galley, S. S.; Shafer, J. C. Elucidating the speciation of extracted lanthanides by diglycolamides. *Coordination Chemistry Reviews* **2023**, *482*, 215071.

(14) Nigond, L.; Musikas, C.; Cuillerdier, C. EXTRACTION BY N, N, N', N-TETRAALKYL-2 ALKYL PROPANE-1, 3 DIAMIDES. I. H2O, HNO3 and HClO4. *Solvent Extraction and Ion Exchange* **1994**, *12*, 261–296.

(15) Condamines, N.; Musikas, C. THE EXTRACTION BY N, N-DIALKYLAMIDES. I. HNO3 AND OTHER INORGANIC ACIDS. *Solvent extraction and ion exchange* **1988**, *6*, 1007–1034.

(16) Bell, K.; Geist, A.; McLachlan, F.; Modolo, G.; Taylor, R.; Wilden, A. Nitric acid extraction into TODGA. *Procedia Chemistry* **2012**, *7*, 152–159.

(17) Singh, M. B.; Patil, S. R.; Lohi, A. A.; Gaikar, V. G. Insight into nitric acid extraction and aggregation of N, N, N', N'-Tetraoctyl diglycolamide (TODGA) in organic solutions by molecular dynamics simulation. *Separation Science and Technology* **2018**, *53*, 1361–1371.

(18) Lommelen, R.; Binnemans, K. Molecular thermodynamic model for solvent extraction of mineral acids by tri-n-butyl phosphate (TBP). *Separation and Purification Technology* **2023**, *313*, 123475.

(19) Acher, E.; Dumas, T.; Tamain, C.; Boubals, N.; Solari, P. L.; Guillaumont, D. Inner to outer-sphere coordination of plutonium (IV) with N, N-dialkyl amide: influence of nitric acid. *Dalton Transactions* **2017**, *46*, 3812–3815.

(20) Hall, G. B.; Campbell, E. L.; Bessen, N. P.; Graham, T. R.; Cho, H.; RisenHuber, M.; Heller, F. D.; Lumetta, G. J. Extraction of Nitric Acid and Uranium with DEHiBA under High Loading Conditions. *Inorganic Chemistry* **2023**, *62*, 6711–6721.

(21) Spjuth, L.; Liljenzin, J.; Hudson, M.; Drew, M.; Iveson, P.; Madic, C. Comparison of extraction behaviour and basicity of some substituted malonamides. *Solvent Extraction and Ion Exchange* **2000**, *18*, 1–23.

(22) Keder, W.; Wilson, A. Amines as extractants—studies of the organic phase. *Nuclear Science and Engineering* **1963**, *17*, 287–297.

(23) Das, N.; Lahiri, S. Liquid-liquid extraction of trace level niobium and tantalum by trioctylamine. *Analytical sciences* **1992**, *8*, 317–322.

(24) Ding, H.; Niu, Y.; Xu, Y.; Yang, W.; Yuan, S.; Qin, Z.; Wu, X. Liquid-liquid extraction of protactinium (V) using tri-iso-octylamine. *Journal of radioanalytical and nuclear chemistry* **2007**, *272*, 263–266.

(25) Sato, T. The extraction of uranyl nitrate from nitric acid solutions by tributyl phosphate. *Journal of Inorganic and Nuclear Chemistry* **1958**, *6*, 334–337.

(26) Alcock, K.; Best, G.; Hesford, E.; McKay, H. Tri-n-butyl phosphate as an extracting solvent for inorganic nitrates—V: Further results for the tetra-and hexavalent actinide nitrates. *Journal of Inorganic and Nuclear Chemistry* **1958**, *6*, 328–333.

(27) Baroncelli, F.; Scibona, G.; Zifferero, M. The extraction of hexavalent uranium from nitric acid solutions by tri-n-dodecylamine nitrate. *Journal of Inorganic and Nuclear Chemistry* **1962**, *24*, 547–559.

(28) Nukada, K.; Naito, K.; Maeda, U. On the mechanism of the extraction of uranyl nitrate by tributyl phosphate II. Infrared Study. *Bulletin of the Chemical Society of Japan* **1960**, *33*, 894–898.

(29) Tan, B.; Chang, C.; Xu, D.; Wang, Y.; Qi, T. Modeling of the competition between uranyl nitrate and nitric acid upon extraction with tri-n-butyl phosphate. *ACS omega* **2020**, *5*, 12174–12183.

(30) Puzikov, E.; Zilberman, B. Y.; Goletskii, N.; Blazheva, I.; Kudinov, A. Use of a Unified Model with TBP Dilution for Describing the Extraction of Nitric Acid and Hexavalent Actinide Nitrates in Multicomponent Nitrate Systems. *Radiochemistry* **2019**, *61*, 554–561.

(31) Ferraro, J. R.; Borkowski, M.; Chiarizia, R.; McAlister, D. R. FT-IR spectroscopy of nitric acid in TBP/octane solution. *Solvent Extraction and Ion Exchange* **2001**, *19*, 981–992.

(32) Servis, M. J.; Wu, D. T.; Braley, J. C. Network analysis and percolation transition in hydrogen bonded clusters: nitric acid and water extracted by tributyl phosphate. *Physical Chemistry Chemical Physics* **2017**, *19*, 11326–11339.

(33) Ivanov, P.; Mu, J.; Leay, L.; Chang, S.-Y.; Sharrad, C.; Masters, A.; Schroeder, S. Organic and third phase in HNO3/TBP/n-dodecane system: No reverse micelles. *Solvent Extraction and Ion Exchange* **2017**, *35*, 251–265.

(34) Lewis, N. H.; Fournier, J. A.; Carpenter, W. B.; Tokmakoff, A. Direct observation of ion pairing in aqueous nitric acid using 2D infrared spectroscopy. *The Journal of Physical Chemistry B* **2018**, *123*, 225–238.

(35) de la Puente, M.; David, R.; Gomez, A.; Laage, D. Acids at the Edge: Why Nitric and Formic Acid Dissociations at Air–Water Interfaces Depend on Depth and on Interface Specific Area. *Journal of the American Chemical Society* **2022**, *144*, 10524–10529.

(36) Ye, X.; Cui, S.; Almeida, V. d.; Khomami, B. Interfacial complex formation in uranyl extraction by tributyl phosphate in dodecane diluent: a molecular dynamics study. *The Journal of Physical Chemistry B* **2009**, *113*, 9852–9862.

(37) Sahu, P.; Ali, S. M.; Shenoy, K. T. Passage of TBP–uranyl complexes from aqueous–organic interface to the organic phase: insights from molecular dynamics simulation. *Physical Chemistry Chemical Physics* **2016**, *18*, 23769–23784.

(38) Kusaka, R. Liquid interfaces related to lanthanide and actinide chemistry studied using vibrational sum frequency generation spectroscopy. *Journal of Nuclear and Radiochemical Sciences* **2020**, *20*, 28–31.

(39) Chen, S.; Li, Z.; Voth, G. A. Acidic Conditions Impact Hydrophobe Transfer across the Oil–Water Interface in Unusual Ways. *The Journal of Physical Chemistry B* **2023**, *127*, 3911–3918.

(40) Verstegen, J. Distribution of nitric acid between water and organic solvents containing tri-n-octyl amine. *Transactions of the Faraday Society* **1962**, *58*, 1878–1888.

(41) Baroncelli, F.; Scibona, G.; Zifferero, M. The extraction of nitric acid by long chain tertiary amines. *Journal of Inorganic and Nuclear Chemistry* **1962**, *24*, 405–413.

(42) Verstegen, J. Distribution of nitric acid between water and organic solvents, containing tri-n-octyl amine—II. *Journal of Inorganic and Nuclear Chemistry* **1964**, *26*, 1085–1102.

(43) Gourisse, D. *Mechanism of the extraction of nitric acid and water by organic solutions of tertiary alkyl-amines*; 1966.

(44) Sinitsyn, N.; Buslaeva, T.; Kartsev, G.; Ignat'eva, S.; Egorova, N. The dipole moments and association of tri-n-octylammonium salts in solution. *Theoretical and Experimental Chemistry* **1978**, *14*, 301–306.

(45) Fomin, V.; Potapova, V. Extraction of nitric acid with amines. *Russian Journal of Inorganic Chemistry* **1963**, *08*, 509–516.

(46) Bac, R. The extraction of excess nitric acid and water by tri-(long-chain)-alkyl amine nitrates in organic diluents. *Journal of Inorganic and Nuclear Chemistry* **1970**, *32*, 3655–3666.

(47) Sadhu, B.; Clark, A. E. Modulating Aggregation in Microemulsions: The Dispersion by Competitive Intermolecular Interaction Model. *The Journal of Physical Chemistry Letters* **2022**, *13*, 10981–10987.

(48) Sadhu, B.; Clark, A. E. Molecular dynamics and network analysis reveal the contrasting roles of polar solutes within organic phase amphiphile aggregation. *Journal of Molecular Liquids* **2022**, *359*, 119226.

(49) Servis, M. J.; Piechowicz, M.; Soderholm, L. Impact of water extraction on malonamide aggregation: A molecular dynamics and graph theoretic approach. *The Journal of Physical Chemistry B* **2021**, *125*, 6629–6638.

(50) Annapureddy, H. V.; Kashyap, H. K.; De Biase, P. M.; Margulis, C. J. What is the origin of the prepeak in the X-ray scattering of imidazolium-based room-temperature ionic liquids? *The Journal of Physical Chemistry B* **2010**, *114*, 16838–16846.

(51) Lovrincevic, B.; Pozar, M.; Jukic, I.; Perera, A. Role of Charge Ordering in the Dynamics of Cluster Formation in Associated Liquids. *The Journal of Physical Chemistry B* **2023**, *127*, 5645–5654.

(52) Hayes, R.; Warr, G. G.; Atkin, R. Structure and nanostructure in ionic liquids. *Chemical reviews* **2015**, *115*, 6357–6426.

(53) Griffin, P. J.; Holt, A. P.; Wang, Y.; Novikov, V. N.; Sangoro, J. R.; Kremer, F.; Sokolov, A. P. Interplay between hydrophobic aggregation and charge transport in the ionic liquid methyltrioctylammonium bis (trifluoromethylsulfonyl) imide. *The Journal of Physical Chemistry B* **2014**, *118*, 783–790.

(54) Knight, A. W.; Chiarizia, R.; Soderholm, L. Extraction selectivity of a quaternary alkylammonium salt for trivalent actinides over trivalent lanthanides: does Extractant aggregation play a role? *Solvent Extraction and Ion Exchange* **2017**, *35*, 266–279.

(55) Lu, Z.; Dourdain, S.; Dufrêche, J.-F.; Demé, B.; Zemb, T.; Pellet-Rostaing, S. Effect of alkyl chains configurations of tertiary amines on uranium extraction and phase stability–part II: Curvature free energy controlling the ion transfer. *Journal of Molecular Liquids* **2022**, *349*, 118487.

(56) Baldwin, A. G.; Servis, M. J.; Yang, Y.; Bridges, N. J.; Wu, D. T.; Shafer, J. C. The structure of tributyl phosphate solutions: Nitric acid, uranium (VI), and zirconium (IV). *Journal of Molecular Liquids* **2017**, *246*, 225–235.

(57) Servis, M. J.; Nayak, S.; Seifert, S. The pervasive impact of critical fluctuations in liquid–liquid extraction organic phases. *The Journal of Chemical Physics* **2021**, *155*.

(58) Bac, R. The extraction of excess nitric acid and water by tri-(long-chain)-alkyl amine nitrates in organic diluents. *Journal of Inorganic and Nuclear Chemistry* **1970**, *32*, 3655–3666.

(59) Verstegen, J. M. The extraction of nitric acid by tri-n-octyl amine. *Journal of Inorganic and Nuclear Chemistry (England) Merged with Inorg. Nucl. Chem. Lett. to form Polyhedron* **1964**, *26*, 2311.

(60) Torii, H.; Watanabe, K. Asymmetry of the Electrostatic Environment as the Origin of the Symmetry Breaking Effect of the Nitrate Ion in Aqueous Solution. *The Journal of Physical Chemistry B* **2023**, *127*, 6507–6515.

(61) Fumino, K.; Fossog, V.; Stange, P.; Paschek, D.; Hempelmann, R.; Ludwig, R. Controlling the subtle energy balance in protic ionic liquids: Dispersion forces compete with hydrogen bonds. *Angewandte Chemie International Edition* **2015**, *54*, 2792–2795.

(62) Perera, A. From solutions to molecular emulsions. *Pure and Applied Chemistry* **2016**, *88*, 189–206.

(63) Servis, M. J.; Stephenson, G. Mesostructuring in liquid–liquid extraction organic phases originating from critical points. *The Journal of Physical Chemistry Letters* **2021**, *12*, 5807–5812.

(64) Bonnett, B. L.; Sheyfer, D.; Wimalasiri, P. N.; Nayak, S.; Lal, J.; Zhang, Q.; Seifert, S.; Stephenson, G. B.; Servis, M. J. Critical fluctuations in liquid–liquid extraction organic phases controlled by extractant and diluent molecular structure. *Physical Chemistry Chemical Physics* **2023**,

(65) Prevost, S.; Lopian, T.; Pleines, M.; Diat, O.; Zemb, T. Small-angle scattering and morphologies of ultra-flexible microemulsions. *Journal of Applied Crystallography* **2016**, *49*, 2063–2072.

(66) Cabry, C. P.; D'Andrea, L.; Shimizu, K.; Grillo, I.; Li, P.; Rogers, S.; Bruce, D. W.; Canongia Lopes, J. N.; Slattery, J. M. Exploring the bulk-phase structure of ionic liquid mixtures using small-angle neutron scattering. *Faraday Discuss.* **2018**, *206*, 265–289.

(67) Yang, H.; Finlayson-Pitts, B. J. Infrared spectroscopic studies of binary solutions of nitric acid and water and ternary solutions of nitric acid, sulfuric acid, and water at room temperature: Evidence for molecular nitric acid at the surface. *The Journal of Physical Chemistry A* **2001**, *105*, 1890–1896.

(68) Mitra, S.; Yang, N.; McCaslin, L. M.; Gerber, R. B.; Johnson, M. A. Size-Dependent Onset of Nitric Acid Dissociation in Cs+·(HNO3)(H2O) n= 0–11 Clusters at 20 K. *The Journal of Physical Chemistry Letters* **2021**, *12*, 3335–3342.

(69) Lefrançois, L.; Delpuech, J.-J.; Hébrant, M.; Chrisment, J.; Tondre, C. Aggregation and protonation phenomena in third phase formation: An NMR study of the quaternary malonamide/dodecane/nitric acid/water system. *The Journal of Physical Chemistry B* **2001**, *105*, 2551–2564.

(70) Mhanna, R.; Lefort, R.; Noirez, L.; Morineau, D. Microstructure and concentration fluctuations in alcohol–Toluene and alcohol-Cyclohexane binary liquids: A small angle neutron scattering study. *Journal of Molecular Liquids* **2016**, *218*, 198–207.

(71) Teubner, M.; Strey, R. Origin of the scattering peak in microemulsions. *The Journal of Chemical Physics* **1987**, *87*, 3195–3200.

(72) Frisch, M. J. et al. Gaussian˜16 Revision C.01. 2016; Gaussian Inc. Wallingford CT.

TOC Graphic